JOURNAL OF MATERIALS SCIENCE 24 (1989) 693–697

Roles of precipitates on corrosion fatigue crack growth of high-strength steels in corrosive environments

R. HAMANO
High Strength Materials Division, National Research Institute for Metals, Sengen, Sakura-mura, Niihari-gun, Ibaragi-ken 305, Japan

The effect of microstructures on resistance to corrosion fatigue cracking and fracture surface morphology for age-hardened steels were investigated in a 3.5% NaCl aqueous solution under a cathodic potential of −0.85 V (Ag/AgCl). The free corrosion was about −0.63 V (Ag/AgCl). The resistance to corrosion fatigue cracking of materials containing coherent precipitates in the matrix (underaged conditions) was less than that of materials containing incoherent precipitates (reheated conditions) at equal strength levels. Accelerated fatigue crack growth rates of the underaged material in the aqueous solution were followed by cracking along prior-austenite grain boundaries, due to hydrogen embrittlement, while the overaged material did not show accelerated fatigue crack growth rates and had fracture surfaces similar to those in air. The difference in the fracture surfaces of both materials in air and in the aqueous solution was considered to depend on the ease of diffusion of hydrogen to the prior-austenite grain boundaries. It is concluded that incoherent precipitates in the matrix made hydrogen accumulation at prior-austenite grain boundaries much slower than for coherent precipitates.

1. Introduction

In many structural components the failure by corrosion fatigue tends to occur with increasing strength when they are exposed in corrosive environments under cyclic loading. Thus, it is important to understand the fatigue crack propagation behaviour of structural materials in service environments.

Komai *et al.* [1] reported that the fatigue crack growth of high-strength steel in 1% NaCl aqueous solution were explained in terms of a stress-dissolution mechanism, hydrogen embrittlement, and wedge-effects induced by corrosion products. Usually steel components are cathodically protected against corrosion. Under the conditions of cathodic protection, corrosion fatigue crack growth rates of steels might be enhanced due to hydrogen embrittlement rather than stress-assisted dissolution.

Recent fractographic studies on high-strength steels [2] indicated that the acceleration of crack growth rates due to hydrogen embrittlement is accompanied by a change in fracture surface morphology, namely, from ductile transgranular in air to intergranular or brittle cleavage failure mode. However, the correlation of a change in fracture surface morphology due to hydrogen embrittlement with microstructures of the materials has not yet been elucidated.

The effect of microstructures on a change in fracture surface morphology due to hydrogen embrittlement and on corrosion fatigue crack growth behaviour of high-strength steels could be investigated under cathodic polarization in a corrosive environment in order to improve the resistance to corrosion fatigue cracking.

In the present study, the response of different microstructures of high-strength steels to fatigue crack growth rates and the accompanied change of fracture surface morphology were investigated under cathodic polarization in a 3.5% aqueous solution, using age-hardenable high-strength steels.

2. Experimental procedure

The materials used in the study were melted in a vacuum induction furnace. The chemical composition of the steels is shown in Table I. After hot forming, the 10 mm thick plates were austenitized at 1100° C for 30 min, water quenched, and tempered as follows. The materials 1UN or 3UN were tempered at 510° C for 1 h and material 3OV was tempered at 510° C for 1 h after reheating at 750° C for 20 min. The materials 1UN and 3UN had precipitates of carbides and NiAl, both of which were coherent with the matrix [3]. Material 3OV had incoherent carbides and coherent NiAl precipitates with the matrix. The mechanical properties at room temperature are given in Table II.

TABLE I Chemical composition (wt %)

Material	Ni	Al	Cr	Mo	Mn	C	P	S
1UN	5.20	0.65	1.63	1.58	0.19	0.14	0.017	0.005
3UN, 3OV	5.07	1.94	1.73	1.55	0.19	0.14	0.018	0.005

0022–2461/89 $03.00 + .12

TABLE II Mechanical properties

Specimens	Yield strength (0.2% offset) (MPa)	Ultimate strength (MPa)	Red. of area (%)
1UN	1053	1271	72.4
3UN	1330	1585	51.3
3OV	1064	1298	71.6

The wedge-opening load type specimens (H/W = 0.98, thickness of 5.0 mm) were cut from the aged plates with notches normal to the rolling direction and a transverse–longitudinal crack plane orientation. Prior to fatigue testing all specimens were pre-cracked at a load ratio of 0.1 in laboratory air. During pre-cracking, the maximum load was lowered in steps of 5% of the maximum load with fatigue crack extensions of 0.4 mm length in each step, using a frequency of 15 Hz. When a fatigue pre-cracking of length 2.5 mm length was attained, subsequent fatigue testing was carried out. After pre-cracking, the applied load range was maintained throughout the fatigue testing. The stress intensity factor solution is given by Novak and Rolfe [4].

The corrosion fatigue tests in a 3.5% NaCl aqueous solution were carried out on a 15 ton closed-loop servo-hydraulic machine, using a load wave of tension–tension sinusoidal shape, a load ratio of 0.1 and a frequency of 5 Hz.

The solution was continually circulated through the cell from a 10 litre capacity reservoir at a flow rate of 0.2 litre min^{-1}. The temperature in the solution was held at 22 $\pm$ 1° C and the solution was renewed once a week. An electrochemical potential of -0.85 V (Ag/AgCl) was applied with a potentiostat using a silver-saturated silver chloride reference electrode. The crack length was measured to an accuracy of 0.01 mm on polished surfaces of the specimens using a travelling microscope. The crack growth rates were calculated from subsequent crack length increment of 0.4 mm.

Fracture surfaces were examined by scanning electron microscopy. The percentage of intercrystalline fracture surfaces was estimated as follows. A set of 25 by 24 lines was drawn on scanning electron micrographs and the number of grid points on the intergranular fracture surfaces was counted. The percentage of intergranular fracture area was calculated using the following equation

$$\mathrm{IG}(\%) = (n/N) \times 100\%$$

where, n is number of grid points on intergranular fracture and N is total number on the grid.

3. Experimental results

Fig. 1 shows the fatigue crack growth rates as a function of stress intensity factor range ΔK, for the tests in air and in aqueous solution under a cathodic potential of -0.85 V (Ag/AgCl). In the tests carried out in the aqueous solution there was a significant dependency of fatigue crack growth rates on microstructures compared with in air. It is obvious that the underaged materials exhibited higher crack growth rates with increasing strength in the aqueous solution

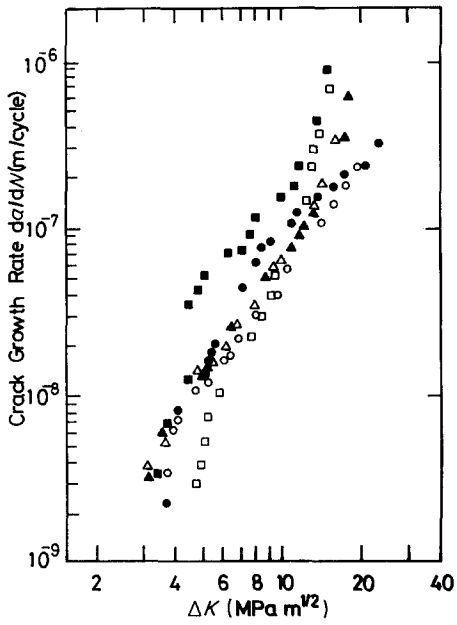

Figure 1 Fatigue crack growth rates for specimens of 1UN, 3UN and 3OV in air (open symbols) and in 3.5% NaCl aqueous solution under a cathodic potential of -0.85 V (Ag/AgCl) (solid symbols) as a function of stress intensity range, ΔK. (○, ●) 1UN, (□, ■) 3UN, (△, ▲) 3OV.

compared with the test in air and that the overaged material, 3OV, had a higher resistance to fatigue cracking for the tests carried out in aqueous solution than the underaged material, 1UN, independent of the fact that both materials had almost similar strengths.

Fig. 2 shows the environmental sensitivity of fatigue crack growth rates of the materials as a function of stress intensity factor range, ΔK. The environmental sensitivity of the crack growth rates is defined as a ratio of crack growth rates in the NaCl aqueous solution, da/dN, to one in air at various stress intensity factor ranges, ΔK. The environmental sensitivities were small at lower ΔK level, and showed a maximum at ΔK of about 6.5 MPa $m^{1/2}$ and decreased at higher

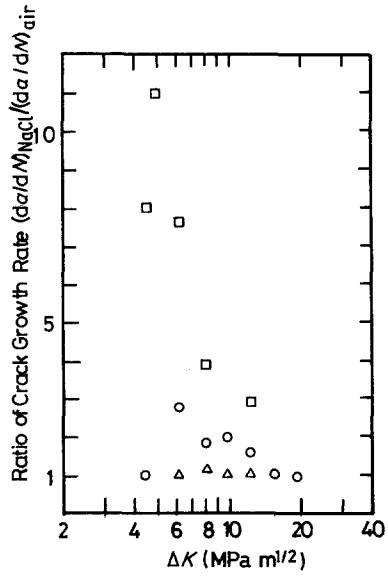

Figure 2 Ratio of crack growth rates in 3.5% NaCl aqueous solution under a cathodic potential of -0.85 V (Ag/AgCl) to ones in air as a function of stress intensity range, ΔK. (○) 1UN, (□) 3UN, (△) 3OV.

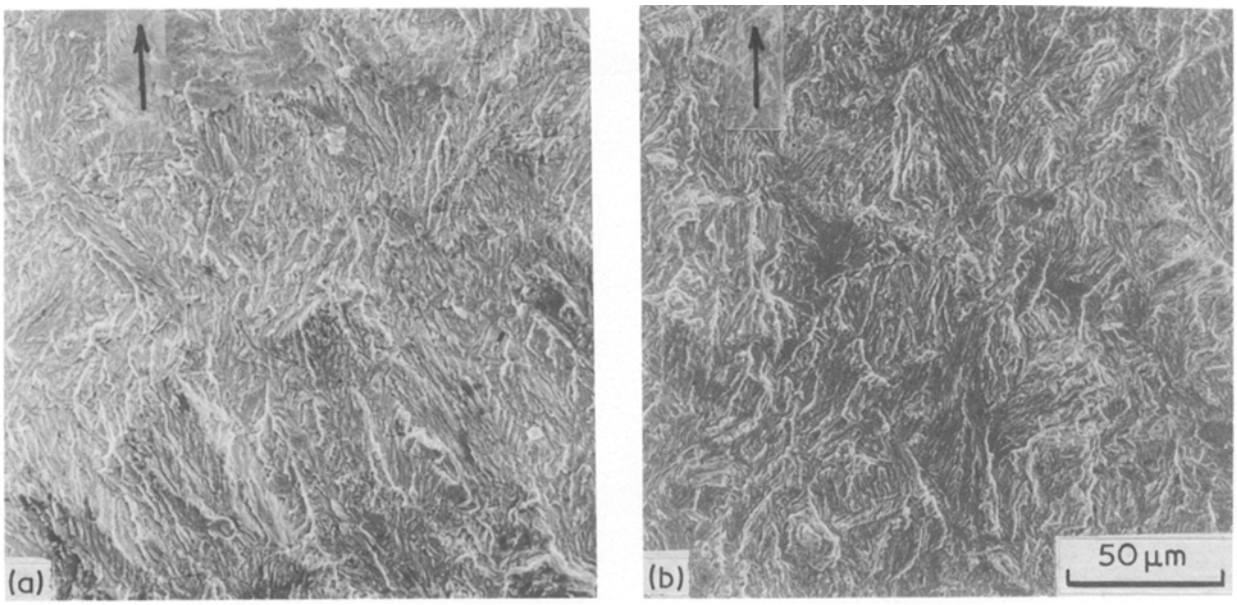

Figure 3 Scanning electron micrographs obtained at $\Delta K = 9.0\,\mathrm{MPa\,m^{1/2}}$ in air: (a) 1UN and (b) 3OV. Arrows show direction of crack propagation.

ΔK levels for all three materials. The environmental sensitivity of material 3OV was small over a variety of stress intensity factor ranges, ΔK, as illustrated in Fig. 2.

Fig. 3 shows the fracture surfaces of the materials 1UN and 3OV fatigued at about $6.5\,\mathrm{MPa\,m^{1/2}}$ of ΔK in air. The fatigue surfaces of all materials in air are characterized by transgranular ductile separation with a small quantity of intercrystalline fracture, and the intercrystalline fracture surfaces are observed much more in material 3UN than in the others. Fig. 4 shows the fracture surfaces fatigued in the aqueous solution at a given ΔK. The fracture surfaces of material 3OV tested in the aqueous solution did not show any significant difference from that tested in air environment at a given ΔK, as can be seen by comparing Figs 3 and 4. The fracture surfaces of materials 1UN and 3UN in the aqueous solution exhibited a brittle appearance characterized by intergranular facets along prior-austenite grain boundaries, implying the effects of hydrogen embrittlement [5]. At higher ΔK levels, the fracture surfaces of 1UN are characterized by ductile transgranular separation similar to that in the air environment.

Fig. 5 shows the percentage of intergranular fracture surfaces for the three materials tested both in air and aqueous environments as a function of ΔK. It is readily seen that the percentage of intergranular fractures in air was below 10% for all these materials. In the aqueous solution, material 3OV had the lowest percentage of intergranular fracture among the three materials. No significant differences in percentage of intergranular fracture for material 3OV tested both in air and the aqueous solution could be observed.

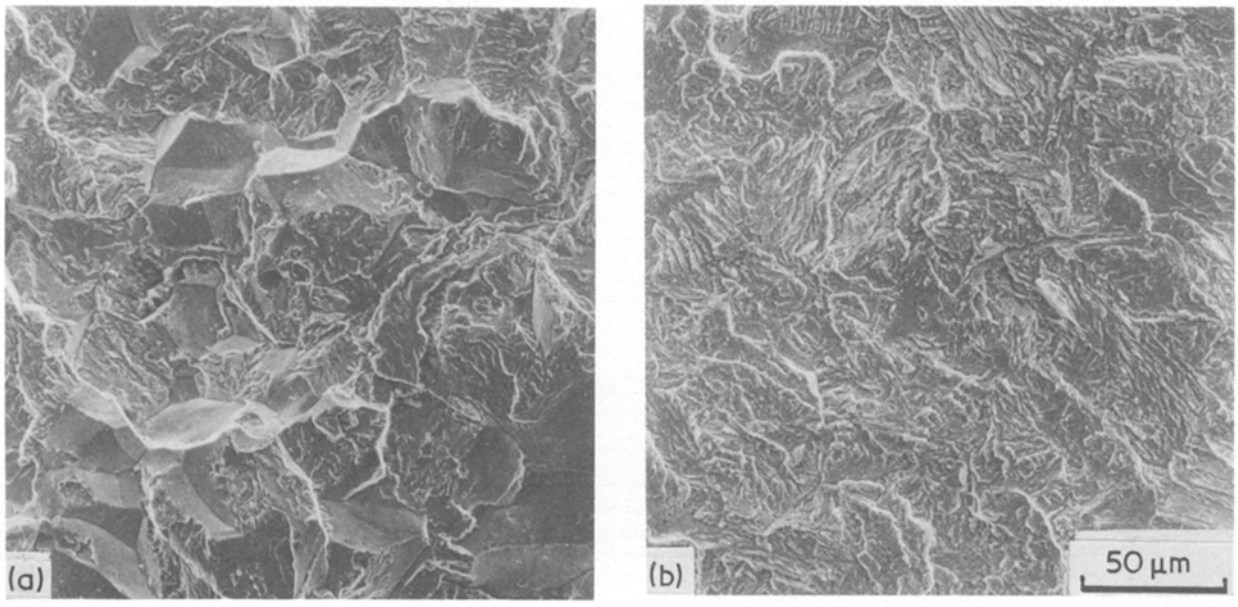

Figure 4 Scanning electron micrographs obtained at $\Delta K = 9.0\,\mathrm{MPa\,m^{1/2}}$ in 3.5% NaCl aqueous solution under cathodic potential of -0.85 V (Ag/AgCl): (a) 1UN and (b) 3OV.

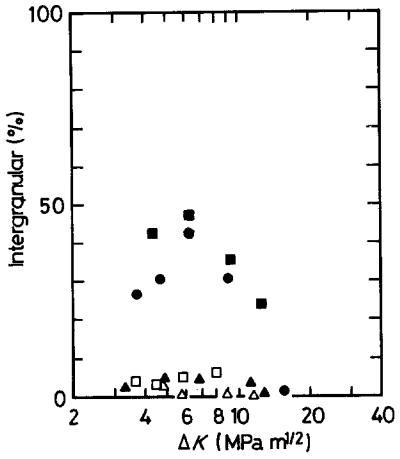

Figure 5 Percentage of intergranular fracture areas in air (open symbols) and in 3.5% NaCl aqueous solution under cathodic potential of −0.85 V (Ag/AgCl) (solid symbols). (●) 1UN, (□, ■) 3UN, (△, ▲) 3OV.

Material 3UN had the highest percentage of intergranular fracture in the aqueous solution. It is observed that the percentage of intergranular fractures for materials 1UN and 3UN could be seen to have a peak at ΔK of about 6.5 MPa $m^{1/2}$.

4. Discussion

It was observed that the environmental susceptibility of fatigue crack growth rates of the age-hardened materials in the NaCl aqueous solution is dependent both on ageing conditions and strength of the materials. For example, the underaged material, 1UN, had the same yield strength as the overaged material, 3OV, and the latter showed better resistance to corrosion fatigue cracking in the aqueous solution than the former did.

The most important effects of ageing treatments on microstructures are summarized in Table III, but the effect of microstructures upon fatigue crack growth behaviour might be very complex, especially in the aqueous solution. In view of the presence of predominant intergranular mode due to environment-assisted fatigue cracking of the present steels, it is reasonable to presume that the embrittlement mechanism involves hydrogen-induced decohesion along prior-austenite grain boundaries. Therefore, environmental enhancement of fatigue crack growth rates would be dependent on the ease of cracking through prior-austenite grain boundaries caused by hydrogen.

When mode II displacement exists at lower stress intensity ranges [6] fatigue crack growth rates are decreased due to roughness-induced crack closure. A previous paper [3] showed that underaged conditions increased crack closure more than overaged conditions in air, because of enhanced mode II deformation. In a corrosive environment, accelerated fatigue cracking due to hydrogen embrittlement propagates more easily in mode I opening, normal to the plane with maximum principle stress, rather than in mode II shear deformation [7]. Therefore, the difference in environmental sensitivity of fatigue crack growth rates between underaged and overaged conditions could not be explained only from a concept of homogeneous or inhomogeneous plastic deformation behaviours accompanied by ageing treatments.

Thus, it might be reasonable to suppose that the mechanism responsible for fatigue crack acceleration in the aqueous solution depends on the partitioning or diffusion of hydrogen to the prior-austenite grain bondaries. The separation along prior-austenite grain boundaries would occur more easily with increasing hydrogen content at these boundaries. It is obvious that the partitioning or diffusion of hydrogen to prior-austenite grain boundaries might be affected by the microstructures within the prior-austenite grain if the grain sizes were not changed by heat treatments. The characteristics of the microstructures of materials 1UN and 3OV are shown in Table III. Because the prior-austenite grain sizes of these materials are almost the same, the microstructures affecting diffusion of hydrogen to the grain boundaries could be considered to exist within the grains.

The decrease of partitioning of hydrogen in the grain boundaries will occur if hydrogen is trapped within the grains, and leads to the decrease of cracking rates along prior-austenite grain boundaries. The microstructures within the grains such as (1) precipitates, (2) dislocations, (3) lath boundaries, could be considered to be effective trap sites. As pointed out by Pressouyre and Bernstein [8], precipitates coherent with the matrix act as weaker trap sites (reversible traps), while precipitates incoherent with the matrix act as strong trap sites (irreversible traps). It is obvious that coherent precipitates are easily saturated with hydrogen and will exchange hydrogen with other stronger traps. As incoherent precipitates have higher trapping energy of hydrogen, they will not release trapped hydrogen. This character of irreversible traps is retained during a test involving deformation because the interface between the precipitates and the matrix grows and increases its trapping capacity, where traps will not become saturated [9]. Therefore, judging from above considerations of the roles of precipitates as hydrogen traps, hydrogen accumulation at prior-austenite grain boundaries will be delayed much more in the material having incoherent precipitates than in the material containing coherent precipitates. Also, material 1UN had many more

TABLE III Characteristics of microstructures

Specimens	Precipitates	Width of lath boundary (μm)	Dislocation density	Prior austenite grain size (μm)
1UN	M_2C	0.20	high	31.2
3UN	M_2C, NiAl		high	23.0
3OV	M_2C, NiAl	0.26	low	27.1

dislocations than material 3OV. Dislocations will act as hydrogen traps and transport hydrogen to fracture sites. Such a hydrogen transport by dislocations has already been proposed by Tien *et al.* [10]. However, because dislocation-aided transport of hydrogen is larger than the diffusion rate of hydrogen and the crack advance per cycle [11], it can be dismissed.

Lath boundaries, which consisted of low-angle boundaries, will not be so effective in the trapping of hydrogen as are the incoherent precipitates. As shown in Table III, the difference in the lath size between materials 1UN and 3OV was not large. Therefore, in the present study the effect of lath boundaries on corrosion fatigue crack growth rates could be considered to be small.

Following the above context, it is understood that material 3OV could have a higher resistance to cracking along prior-austenite grain boundaries at the same applied stress intensity factor range than material 1UN. As shown in Fig. 2, the marked reduction of environmental enhancement of fatigue crack growth rates at higher crack growth rates occurred because the hydrogen atoms can no longer diffuse rapidly to keep up with the crack tip which is continuously advancing by mechanical fatigue. Also the marked reduction in environmental enhancement at slow fatigue crack growth rates could be observed, because under cathodic potential, fatigue crack growth enhancement due to dissolution is not possible and adsorption or entry of hydrogen into the matrix from crack surfaces is difficult. Several investigators reported that the corrosion fatigue crack growth rates under cathodic potential conditions decrease with decreasing ΔK and approach or intersect air data at lower ΔK levels near the threshold. In the present study the above mentioned results were obtained under cathodic potential as shown in Fig. 3. According to Komai *et al.* [1], the rate-controlling step at a stress intensity factor ΔK near the threshold factor ΔK, is the exposure of a clean surface at the crack tip. Therefore, it can be understood that the effects of microstructures on the fatigue crack growth enhancement due to hydrogen embrittlement decreased under cathodic potential conditions at lower ΔK levels.

5. Conclusions

1. For age-hardened high-strength materials, fatigue crack growth resistance under a cathodic potential of -0.85 V (Ag/AgCl) in the aqueous solution was dependent on ageing conditions. The acceleration of fatigue crack growth was larger in underageing conditions than in overageing conditions due to hydrogen embrittlement.

2. The fracture stress of underaged materials showed a brittle appearance characterized by intergranular facets along by prior-austenite grain boundaries, implying the effects of hydrogen embrittlement. The overaged condition has the smallest ratio of intergranular fracture surfaces.

3. The acceleration of fatigue crack growth in the aqueous solution under cathodic protection was dependent on diffusion of hydrogen into prior-austenite grain boundaries. Hydrogen accumulation at the grain boundaries was delayed much more in the overaged conditions having incoherent precipitates than in the underaged conditions having coherent precipitates with the matrix.

Acknowledgements

The authors thank Drs T. Suzuki and A. Ohta for helpful discussion and generous help with the crack closure measurements.

References

1. K. KOMAI, S. KITA and E. ENDO, *Bull. Soc. Mech. Eng.* **49** (1983) 1029.
2. S. YONEZAWA, K. YAMAKAWA and S. YOSHIZAWA, *J. Soc. Mater. Jpn* **33** (1984) 191.
3. R. HAMANO, *Metall. Trans. A* **19A** (1988) 1461.
4. S. R. NOVAK and S. T. ROLFE, *J. Mater.* **4** (1969) 701.
5. R. RUNGTA and J. A. BEGLEY, *Metall. Trans. A* **11A** (1980) 821.
6. R. O. RITCHIE and S. SURESH, *ibid.* **13A** (1982) 937.
7. T. D. LEE, T. GOLDENBERG and J. P. HIRTH, *ibid.* **10A** (1979) 439.
8. G. M. PRESSOUYRE and J. M. BERNSTEIN, *Acta Metall.* **27** (1979) 89.
9. G. M. PRESSOUYRE, *ibid.* **28** (1980) 895.
10. J. K. TIEN, A. W. THOMPSON, I. M. THOMPSON, I. M. BERNSTEIN and R. J. RICHARDS, *Metall. Trans. A* **7A** (1976) 821.
11. J. P. HIRTH, *ibid.* **11A** (1980) 861.

Received 28 December 1987
and accepted 6 May 1988